DOI 10.1007/s11182-024-03141-0
Russian Physics Journal, Vol. 67, No. 4, April, 2024

INFLUENCE OF BIMETAL STRUCTURE AND PHASE COMPOSITION ON LOCALIZED PLASTIC STRAIN

D. V. Orlova, G. V. Shlyakhova, L. V. Danilova, and M. V. Nadezhkin UDC 539.213; 669.017

The paper investigates the macrolocalization of plastic strain due to uniaxial loading of low carbon/austenitic stainless steel produced by electron-beam additive manufacturing followed by annealing at different temperatures. The stress-strain curve of the bimetallic composite is described by the parabolic law. Due to annealing in the range of 350 to 650°C, the yield strength reduces, while strain-to-failure grows as compared to the as-built composite. Localized plastic strain follows the stress-strain curve in all composite states and layers. At the parabolic hardening stage, the formation of a stationary dissipative system of localized plasticity occurs at strain hardening of 0.5. When strain hardening is ≤0.5, a high-amplitude deformation zone appears in the transition layer, which coincides with the site of eventual fracture.

Keywords: additive manufacturing, austenitic stainless steel, heterogeneous microstructure, localized strain, digital image correlation.

INTRODUCTION

In recent years, protective coatings have attracted much attention from research teams. Bimetal comprising low carbon steel and stainless austenitic steel shows good corrosion resistance, high mechanical strength, and can be used to manufacture highly loaded parts operating in corrosive environments. Additive manufacturing is one of the promising methods of fabricating bimetallic parts, implying layer-by-layer melting of powdered or wire material deposited using electric arc, plasma, laser and electron beam [1–4]. Based on this technology, specified properties of various composite materials can be controlled by the composition and process parameters. The development of new production techniques raises the question, how the inhomogeneous structure and phase composition of multilayer materials affect their deformation behavior. A particularly important issue is the influence of phase boundaries on the plastic strain and fracture of material. Digital image correlation (DIC) combined with mechanical strength testing is a good tool for studying various materials, including those fabricated by additive manufacturing [5–8]. The strain evolution is studied on specimens cut in different directions from workpieces disregarding the steel/substrate interface. In this study, we determine strain field components at the interface between austenitic stainless steel layers deposited along the axis of tension and the low carbon steel substrate.

In works [9–11], it was shown that even single crystals and materials with the homogeneous structure were prone to the formation of localized strain zones induced by loading. Depending on the plastic flow stage, macrolocalization of plastic strain occurred either as a separate switching wave in the case of Lüders bands, or stationary localized periodic patterns at the parabolic strain hardening stage, or collapse of the autowave at the prefracture stage [9]. Therefore, for the efficient composite fabrication and application, it is necessary to study the kinetics of localized plastic strain in composites comprising two or more metals obtained by additive manufacturing.

Institute of Strength Physics and Materials Science of the Siberian Branch of the Russian Academy of Sciences, Tomsk, Russia, e-mail: dvo@ispms.ru; shgv@ispms.ru; dlv@ispms.ru; mvn@ispms.ru. Original article submitted March 12, 2024.

TABLE 1. Composition of Initial Materials

	C	Si	Mn	Ni	Cr	S	P	Fe
Substrate	0.14–0.22	0.12–0.3	0.4–0.65	<0.3	<0.3	<0.05	<0.04	Balance
Deposited layer	<0.04	<1.0	0.5–2.5	9.0–12.0	18.0–21.0	<0.04	<0.035	Balance

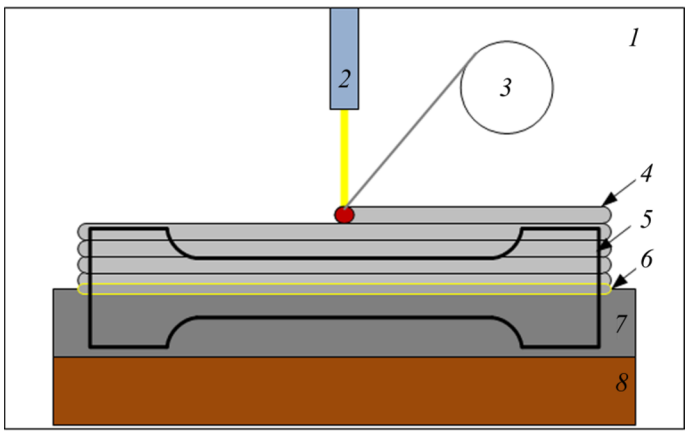

Fig. 1. Schematic of wire-feed EBAM process: *1* – vacuum chamber, *2* – electron gun, *3* – wire feeder, *4* – deposited layer, *5* – dog bone specimen cut, *6* – transition layer, *7* – substrate, *8* – water-cooled copper plate.

The purpose of this work is to examine the kinetics of plastic strain macrolocalization during tension of low carbon/stainless steel composite produced by wire-feed electron beam additive manufacturing in the as-built state and after annealing.

MATERIALS AND METHODS

The steel composite consisting of a low carbon steel substrate 4-mm thick with the austenitic steel layer 5.5-mm thick was used in this experiment. Electron beam additive manufacturing (EBAM) provided the wire deposition in vacuum, as illustrated in Fig. 1. The wire diameter was 1.6 mm. Wire-feed EBAM operating parameters included 27 kV accelerating voltage, 60 mA beam current, $3.8 \cdot 10^{-3}$ m/s feed rate, and 1.3 feed ratio. The chemical composition of the initial materials is given in Table 1.

The dog bone specimens were cut by electrical discharge machining normal to the substrate plane. The specimens had 40 mm gauge length, 8.5 mm width, and 2 mm thickness. The gauge surface exhibited all composite layers, and the deformation process was observed in all layers simultaneously.

Uniaxial tensile tests of dog bone specimens were performed on an AG LFM-125 Testing Machine (Walter + Bai) at $8.33 \cdot 10^{-5}$ s^{-1} strain rate at room temperature. Tensile strength testing was conducted for not annealed (initial state) specimens and those annealed at 350, 450, 550 and 650°C with a 30-min exposure in an atmospheric pressure kiln followed by cooling.

Localized strain zones were identified by sequentially recorded digital images of deformed specimens. For the speckle pattern generation, the gauge surface was illuminated with coherent light using a semiconductor laser (635 nm, 15.0 mW). Speckle patterns of the obtained images were superimposed by recording with a FL3-GE-50S5M-C digital camera (Point Grey Research, Inc., Richmond, British Columbia) with 2448 × 2048 pixels resolution and shooting 5 frames per second. The camera was placed at a 0.3 m distance from the specimen to provide 20.4 μm pixels. The obtained series of images was processed posteriori by DIC [5] to measure the field displacement, strain components, and strain rate. The microhardness testing was performed on a PMT-3M Vickers hardness tester (Russia).

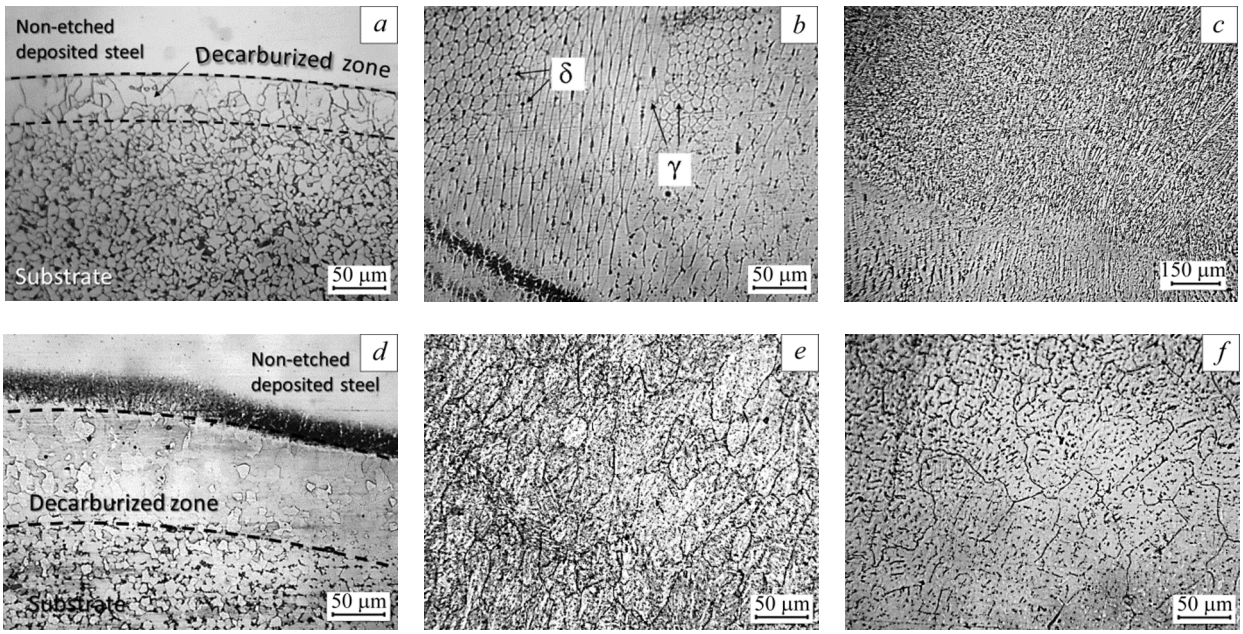

Fig. 2. Composite microstructure of the substrate, first deposited layer, and second layer in as-bult specimen (*a*–*c*) and after 650°C annealing (*d*–*f*).

RESULTS AND DISCUSSION

Microstructure and mechanical properties

Figure 2 contains optical images of the heterogeneous microstructure of wire-feed EBAM-fabricated low carbon/stainless austenitic steel composite. The substrate material of the as-built specimen consists of ferrite grains with the average size of 10.9±1.1 μm and pearlite (Fig. 2*a*). One can see a decarburized zone ~50 μm wide at the steel/substrate interface. After annealing, no changes in the substrate structure are observed, but the width of the decarburized zone changes (Fig. 2*d*). The two-phase microstructure typical for the austenitic steel layers, is represented by light areas of γ-austenite and dark areas of δ-ferrite phases [1, 3]. In the initial state, after the first beam treatment, the formation of the fine-grained austenitic structure is observed at the steel/substrate interface, demonstrating regions with ~10 μm equiaxed grains and ~50 μm elongated grains (Fig. 2*b*). Cellular δ-ferrite locates along the grain boundaries. Further beam motion provides the formation of δ-ferrite dendritic colonies in the austenitic matrix (Fig. 2*c*). The annealing temperature growing from 350 to 650°C, causes partial dissolution of dendritic colonies and the formation of fragments with grain boundaries in the austenitic matrix (Fig. 2*e*, *f*).

The microhardness distribution in bimetal layers is presented in Fig. 3. One can see that after the first beam path, hardening is more pronounced at the steel/substrate interface. As a result of 650°C annealing, the microhardness in the transition zone lowers and continues to gradually decrease in the next layers.

Figure 4 shows stress-strain curves of bimetal specimens and constituent metals obtained by conventional casting, and Table 2 gives their main mechanical properties. These data indicate that as-built bimetal in the initial state has lower ductility and higher strength than cast constituents. The annealing process significantly increases the bimetal ductility. The stress-strain curves can be classified as general, which are usually described by the parabolic function $\sigma = \sigma_0 + K\varepsilon^n$, where K is the strain hardening coefficient and $n \leq 1$ is the strain hardening exponent. Depending on the latter, the following curve stages can be specified: yield plateau ($n = 0$), linear strain hardening ($n = 1$), parabolic strain hardening ($n = 0.5$), and prefracture ($n \leq 0.5$). The duration of these stages is indicated in Table 2.

TABLE 2. Mechanical Properties of Steels and Strain Intervals for Plastic Flow Stages

Steels	Yield point, MPa	Tensile strength, MPa	Elongation to failure	$n = 0$	$n = 1$	$n = 0.5$	$n \leq 0.5$
Low carbon steel	209±4.5	339±4.5	0.30±0.05	0.008–0.022	–	0.028–0.057	0.07–0.28
Austenitic stainless steel	262±3.0	780±5.0	0.70±0.10	–	0.05–0.32	–	0.32–0.69
EBAM-fabricated composite							
Initial state	226±5.0	736±3.5	0.09±0.05	–	–	0.013–0.05	0.05–0.09
350°C	251±5	666	0.21	–	–	0.017–0.18	–
450°C	227±5	642	0.20	–	–	0.02–0.20	–
550°C	217±5	588	0.27	–	–	0.05–0.18	0.18–0.25
650°C	212±5	633	0.30	–	–	0.01–0.19	0.19–0.27

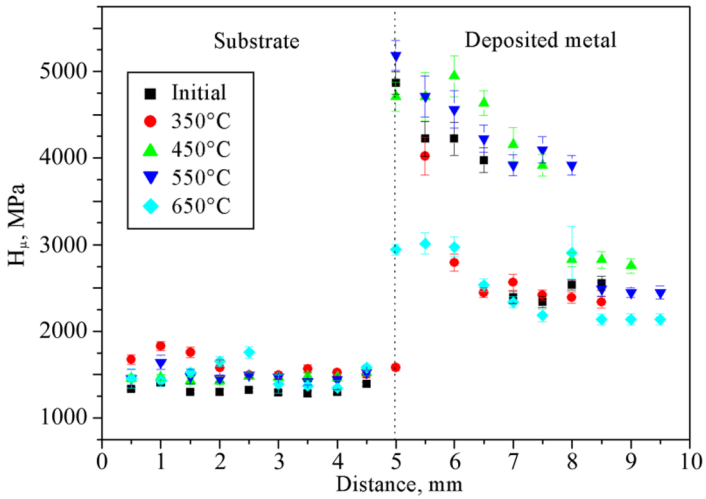

Fig. 3. Microhardness distribution in wire-feed EBAM-fabricated composite.

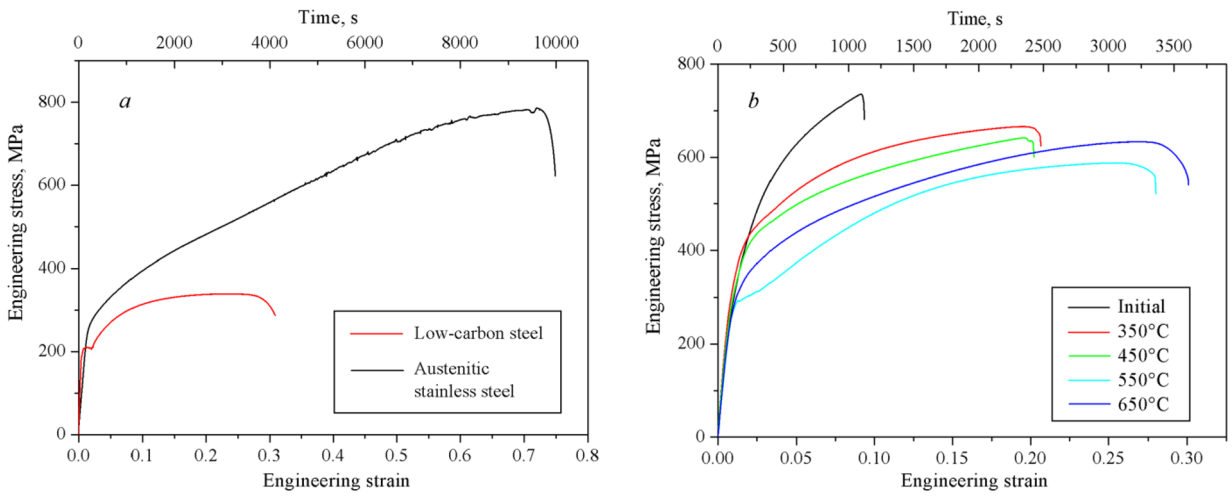

Fig. 4. Stress-strain curves for cast metals (*a*) and EBAM-fabricated composites (*b*).

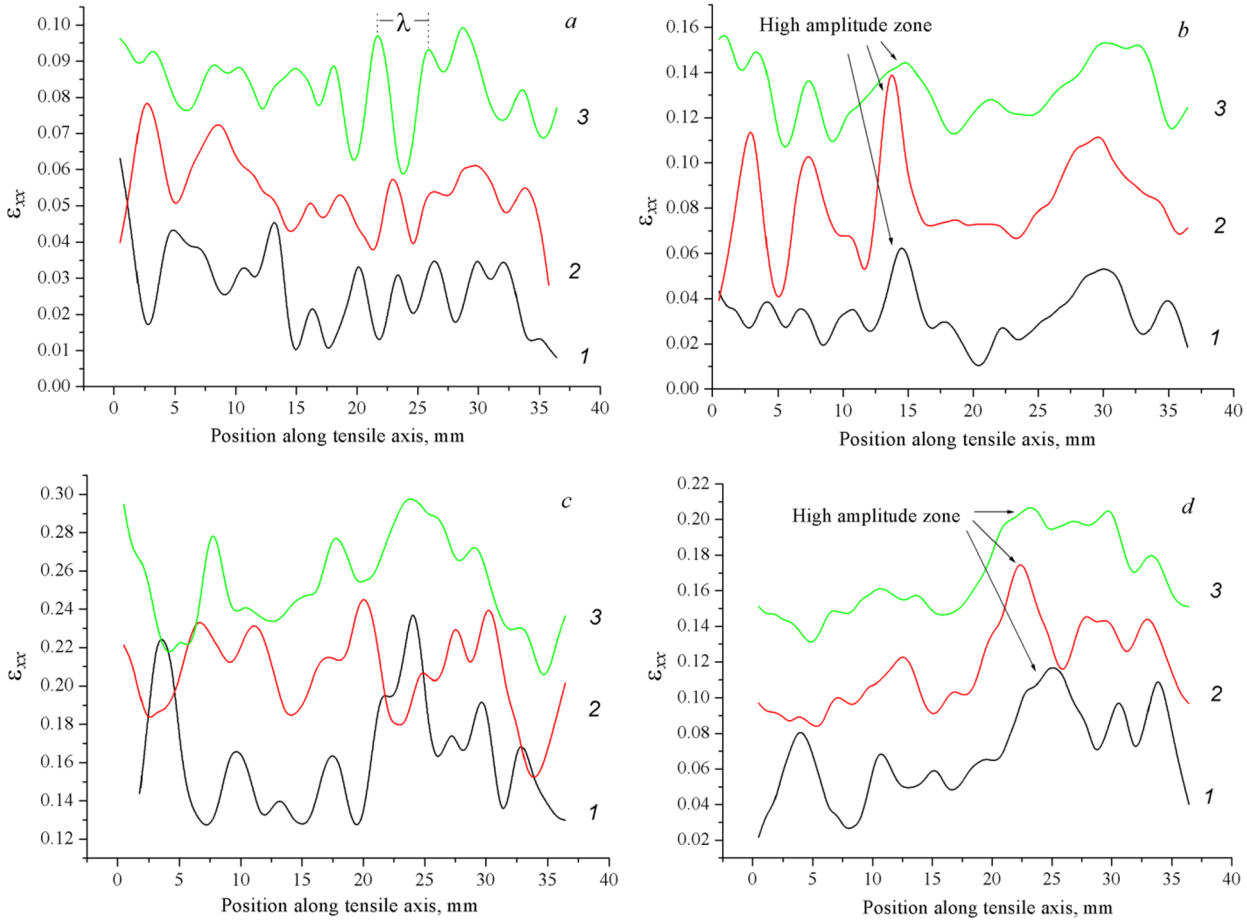

Fig. 5. Total distribution of localized strain $\varepsilon_{xx}(x)$ in composite layers: *1* – substrate, *2* – transition layer, *3* – deposited metal at parabolic and prefracture stages: *a*, *b* – in the initial state, *c*, *d* – after 650°C annealing. In layers *2* and *3*, ε_{xx} is shifted respectively by 0.05 and 0.1 along *y*-axis relative to layer *1*.

Localized strain distribution

According to the autowave theory, the macrolocalization of plastic strain can change the autowaveform, depending on the stage of the plastic flow [10]. For example, Lüders bands typical for low carbon steels and some other alloys, occur in the yield plateau, while the region of localized plastic strain moves along the axis of tension. According to Danilov *et al*. [11], Lüders band wavefront is switching autowaves, which transfer the deformed medium from metastable (elastic) to stable (plastically deformed) state. At the parabolic hardening stage, the kinetics of localized strain in homogeneous metallic materials corresponds to a stationary periodic distribution of localized zones. The stage preceding fracture matches collapse of the autowave [9, 10].

In this work, stress-strain curves of the EBAM-fabricated bimetal at all states, have no yield plateau despite the large content of low carbon steel (Table 2) in contrast to [13], where it is observed on the curve of the loaded three-layer composite consisting of carbon and stainless steels. Lüders deformation in the form of the localized wavefront inherent to this stage, is not observed also. However, annealed specimens with much higher ductility manifest a long stage of parabolic hardening. Figure 5*a*, *c* shows the total $\varepsilon_{xx}(x)$ distribution in the parabolic hardening range at $n = 0.5$ in each layer in the initial bimetal state and after 650°C annealing. Localized zones of stationary periodic distribution formed in each layer during the deformation process, are similar to those in homogeneous specimens. The same is observed for specimens after annealing at 350 to 550°C. In the autowave model of plasticity, the system of equidistant stationary

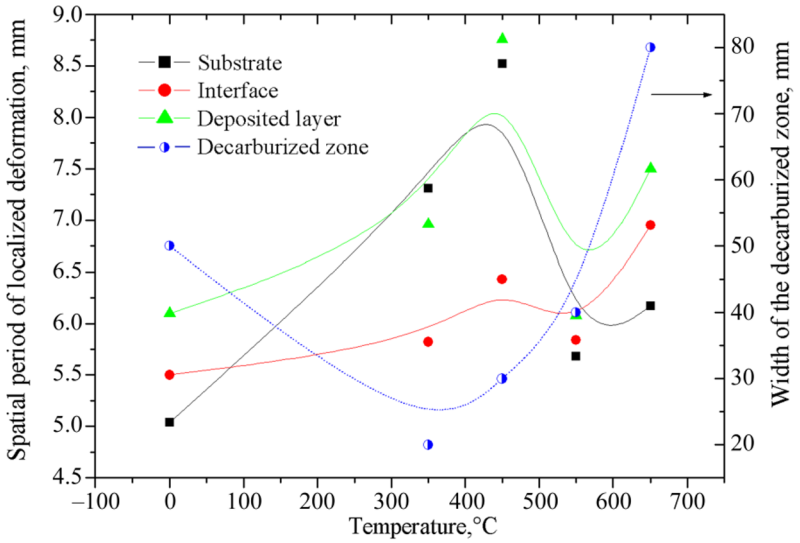

Fig. 6. Temperature dependences of spatial period λ of localized strain in bimetal layers and decarburized zone width.

sites of localized plasticity at the stage of parabolic strain hardening, is interpreted as a stable dissipative structure [10]. In Fig. 6, the spatial period λ of localized strain, which is the distance between localized zones in bimetal layers, depends on the annealing temperature. At the annealing temperature increased up to 450°C, the spatial period grows and is longer at the steel/substrate interface. Maximum λ values correspond to the minimum width of the decarburized zone on the interfacial substrate side.

At the prefracture stage with $n \leq 0.5$ following the parabolic stage, the ε_{xx} amplitude grows in one of the localized strain zones, that eventually coincides with the fracture site (Fig. 5*b*, *d*). The crack initiation site, from which fracture starts, appears in the transition layer. The *x* coordinate of the fracture zone is 15 mm for the initial specimen, and 28 and 24 mm for specimens after 450 and 650°C annealing, respectively. The fracture zone in specimens annealed at 350 and 550°C occurs beyond the strain measurement area.

CONCLUSIONS

This study clearly showed that the stress-strain curve of the low carbon/stainless steel composite fabricated by wire-feed EBAM, was described by the parabolic law. Bimetal annealing in the range of 350 to 650°C, led to a decrease in the yield strength and increase in the strain-to-failure as compared to the as-built specimen. The composite loading in all states suppressed the Lüders deformation. Localized plastic strain occurred in all composite layers during the deformation process.

At the parabolic hardening stage, the formation of the stationary dissipative system of localized plasticity occurred at strain hardening of 0.5. After annealing, maximum values of the localized spatial period corresponded to the minimum width of the decarburized zone at the substrate interface. When strain hardening was ≤0.5, a high-amplitude deformation zone appeared in the transition layer, which coincided with the site of eventual fracture.

COMPLIANCE WITH ETHICAL STANDARDS

Conflicts of interest

The authors declare no conflict of interest.

Financial interests

The authors declare they have no financial interests.

Funding

This research was financially supported by Grant No. 24-29-00580 from the Russian Science Foundation (https://rscf.ru/project/24-29-00580).

Non-financial interests

None.

Acknowledgment

The authors wish to thank the Laboratory of Local Metallurgy in Additive Manufacturing Technologies ISPMS SB RAS for assistance in fabricating composite materials.

REFERENCES

1. W. E. Frazier, J. Mater. Eng. Perform., **23**, 1917–1928 (2014); DOI: 10.1007/s11665-014-0958-z.
2. S. Yu. Tarasov, A. V. Filippov, N. N. Shamarin, *et al*., J. Alloys Compd., **803**, 364–370 (2019); DOI: 10.1016/j.jallcom.2019.06.246.
3. B. Zheng, Y. Zhou, J. Smugeresky, *et al.,* Metall. Mater. Trans. A, **39**, 2237–2245 (2008); DOI: 10.1007/s11661-008-9566-6.
4. E. G. Astafurova, M. Yu. Panchenko, V. A. Moskvina, *et al*., J. Mater. Sci., **55**, 9211–9224 (2020); DOI: 10.1007/s10853-020-04424-w.
5. M. A. Sutton, J. J. Orteu, and H. W. Schreier, Image Correlation for Shape, Motion and Deformation Measurements – Basic Concepts, Theory and Applications, Springer, Berlin (2009); DOI: 10.1007/978-0-387-78747-3.
6. J. Gordon, J. Hochhalter, C. Haden, and D. G. Harlow, Mater. Des., **168**, 107630 (2019); DOI: 10.1016/j.matdes.2019.107630.
7. P. Margerit, D. Weisz-Patrault, K. Ravi-Chandar, and A. Constantinescu, Addit. Manuf., **37**, 101664 (2021); DOI: 10.1016/j.addma.2020.101664.
8. G. Mesmacque, Int. J. Impact Eng., **60**, 107–119 (2013); DOI: 10.1016/j.ijimpeng.2013.04.006.
9. L. B. Zuev, Bull. Russ. Acad. Sci. Phys., **78**, 957–964 (2014); DOI: 10.3103/S1062873814100256.
10. L. B. Zuev, S. A. Barannikova, V. I. Danilov, and V. V. Gorbatenko, Prog. Phys. Met., **22**, No. 1, 3–57 (2021); DOI: 10.15407/ufm.22.01.003.
11. V. I. Danilov, V. V. Gorbatenko, and L. V. Danilova, Steel Transl., **52**, 380–384 (2022); DOI: 10.3103/S0967091222040027.
12. M. V. Nadezhkin, D. V. Orlova, S. A. Barannikova, and L. B. Zuev, Key Eng. Mater., **910**, 849–856 (2022); DOI: 10.4028/p-jc90fe.
13. S. A. Barannikova and Y. V. Li, Russ. Phys. J., **63**, 731–737 (2020); DOI: 10.1007/s11182-020-02091-7.